Published in final edited form as:

Glia. 2023 October ; 71(10): 2323–2342. doi:10.1002/glia.24424.

The expression of ceruloplasmin in astrocytes is essential for postnatal myelination and myelin maintenance in the adult brain

VT Cheli[*],

M Sekhar[*],

DA Santiago González[*],

CG Angeliu,

GE Denaroso,

Z Smith,

C Wang,

PM Paez

Institute for Myelin and Glia Exploration, Department of Pharmacology and Toxicology, Jacobs School of Medicine and Biomedical Sciences, The State University of New York, University at Buffalo, Buffalo, New York.

Abstract

Ceruloplasmin (**Cp**) is a ferroxidase enzyme that is essential for cell iron efflux. The absence of this protein in humans and rodents produces progressive neurodegeneration with brain iron accumulation. Astrocytes express high levels of Cp and iron efflux from these cells has been shown to be central for oligodendrocyte maturation and myelination. To explore the role of astrocytic Cp in brain development and aging we generated a specific conditional KO mouse for Cp in astrocytes (**Cp cKO**). Deletion of Cp in astrocytes during the first postnatal week induced hypomyelination and a significant delay in oligodendrocyte maturation. This abnormal myelin synthesis was exacerbated throughout the first two postnatal months and accompanied by a reduction in oligodendrocyte iron content, as well as an increase in brain oxidative stress. In contrast to young animals, deletion of astrocytic Cp at eight months of age engendered iron accumulation in several brain areas and neurodegeneration in cortical regions. Aged Cp cKO mice also showed myelin loss and oxidative stress in oligodendrocytes and neurons, and at 18 months of age, developed abnormal behavioral profiles, including deficits in locomotion and short-term memory. In summary, our results demonstrate that iron efflux—mediated by astrocytic Cp—is essential for both early oligodendrocyte maturation and myelin integrity in the mature brain. Additionally, our data suggest that astrocytic Cp activity is central to prevent iron accumulation and iron-induced oxidative stress in the aging CNS.

Correspondence to: Pablo M. Paez, Institute for Myelin and Glia Exploration, Department of Pharmacology and Toxicology, Jacobs School of Medicine and Biomedical Sciences, SUNY at Buffalo. NYS Center of Excellence, 701 Ellicott St., Buffalo, New York 14203, USA. Tel: 716-881-7823; Fax: 716-849-6651; ppaez@buffalo.edu.

[*]These authors made equivalent contributions.

Conflict of interest statement: The authors declare no competing financial interests.

Keywords

ceruloplasmin; astrocytes; oligodendrocytes; iron; myelination

INTRODUCTION

Ceruloplasmin (**Cp**) is a ferroxidase enzyme that belongs to the multicopper oxidase family, a group of proteins that utilize copper to oxidize iron (Sato and Gitlin, 1991; Hellman and Gitlin, 2002; Bento et al., 2007). Two distinct isoforms of Cp are produced by alternative splicing in exons 19 and 20: a soluble form and a glycosylphosphatidylinositol (**GPI**) form that is anchored to the cell plasma membrane (Patel et al., 2000). While the soluble isoform is almost entirely synthetized by hepatocytes and accounts for about 95% of the copper found in plasma (Hellman and Gitlin, 2002), the GPI-anchored membrane isoform plays an important role in cellular iron efflux (Muckenthaler et al., 2017) and is expressed by several cell types, including astrocytes, oligodendrocytes, hepatocytes, macrophages, pancreatic, and retinal epithelial cells (Kono et al., 2010; Kono, 2013). Ferrous iron transported out of the cell by ferroportin is safely oxidized by GPI-Cp to facilitate loading on transferrin (**Tf**) (Jeong and David 2003; Miyajima and Hosoi, 2018). Therefore, membrane-bound Cp is essential to ensure non-toxic cell iron release and proper Tf saturation in several tissues (Jeong and David 2003; Miyajima and Hosoi, 2018).

Astrocytes are central players in brain iron homeostasis; they regulate extracellular iron availability in the brain parenchyma and are strategically located to uptake this nutrient from the circulating blood (Amiry-Moghaddam et al., 2003; Simard and Nedergaard, 2004). Astrocytic end-feet processes surround the vasculature of the CNS and are particularly efficient in maintaining the ionic and osmotic homeostasis of the brain (Amiry-Moghaddam et al., 2003; Simard and Nedergaard, 2004). Astrocytes are an essential part of the neurovascular unit in cooperation with brain capillary endothelial cells (BCECs) and pericytes (Abbott et al., 2006; Price et al., 2018) and can transport iron directly from BCECs to neurons and oligodendrocytes (Price et al., 2018). Cp is highly expressed in astrocyte membranes and is fundamental for proper intracellular iron concentration in these cells (Vashchenko and MacGillivray, 2013; Chen et al., 2019). *In vitro*, Cp KO astrocytes exhibit reduced iron efflux, iron overload, and increased free radical production (Chen et al., 2019), indicating that Cp is crucial to prevent iron accumulation in astrocytes and may perform a protective antioxidant function in the developing and adult CNS.

Aceruloplasminemia (**ACp**) is an adult-onset, autosomal recessive disorder, characterized by loss-of-function mutations in the Cp gene (Jeong and David 2006; Miyajima, 2014). ACp's main symptoms include diabetes, retinopathy, liver disease, and progressive neurological symptoms associated with brain iron deposition (Jeong and David 2006; Miyajima, 2014). Brain iron accumulation makes ACp unique in comparison to other systemic iron overload syndromes. Early neurological injury in ACp may be the result of toxic iron release from Cp-deficient cells and the subsequent uptake of non-transferrin bound iron by neurons and oligodendrocytes (Breuer et al., 2000; Jeong and David 2006). In advanced ACp, neurodegeneration and demyelination may be a consequence of iron accumulation and

oxidative damage in neurons and glial cells (Kono and Miyajima, 2006; Kono, 2013; Miyajima and Hosoi, 2018). However, the contribution of astrocytes to these pathological processes has not yet been determined. In this work we present evidence demonstrating that astrocytic Cp is essential for normal oligodendrocyte progenitor cell development and myelination. Additionally, our results indicate that Cp activity in astrocytes is important to prevent demyelination, iron accumulation, and iron-induced oxidative stress in the aging brain. Therefore, this study has clinical implications for neurodegenerative diseases characterized by abnormal brain iron homeostasis.

MATERIALS AND METHODS

Mice Treatment

Mice were housed in the UB Division of Laboratory Animal Medicine vivarium. Procedures were approved by UB's Animal Care and Use Committee and conducted in accordance with the guidelines in "Guide for the Care and Use of Laboratory Animals" from the National Institutes of Health. The $Cp^{tm1a(KOMP)Wtsi}$ "knock-out first allele" mouse (Komp Mouse, # 047193-UCD) was obtained from the Komp Mouse project at UC Davis. The Glast1*Cre*ER^{T2} transgenic mice (Jackson Mice, # 012586), the ROSA26::FLPe knock-in transgenic strain (Jackson Mice, # 009086) and the *Cre* reporter mouse line (Ai9(RCL-tdT) (Jackson Mice, # 007909) were obtained from the Jackson Laboratory. A Cp-floxed ($Cp^{f/+}$) mouse was generated by crossing the $Cp^{tm1a(KOMP)Wtsi}$ mouse with the ROSA26::FLPe knock-in mouse, which express the FLP1 recombinase driven by the Gt(ROSA)26Sor promoter. FLP1 mediated recombination generated a Cp^{tmc1} "conditional ready allele" where the exon 7 of the Cp gene is flanked by loxP sites. Mice with the FRT deletion were backcrossed in C57Bl/6 for 10 generations. Experimental animals were generated by crossing the heterozygous floxed $Cp^{f/+}$ strain with the hemizygous Glast1*Cre*ER^{T2} transgenic line. To delete Cp in Glast1-positive astrocytes, *Cre* activity was induced starting at postnatal day 2 (P2). P2 Glast1-Cp^{KO} ($Cp^{f/f}$, Glast1*Cre*$ER^{Cre/-}$) and control (*Cre*-negative) littermates ($Cp^{f/f}$, Glast1*Cre*$ER^{-/-}$) were intraperitoneally injected once a day for 5 consecutive days with 25mg/kg tamoxifen (Sigma-Aldrich), and brain tissue was collected at P15, P30, and P60. For studies in aged mice, 7 tamoxifen injections of 100mg/kg were administered every other day starting at 8 months and CNS tissue samples were collected at 12 and 18 months of age. For all the experiments presented in this work, mice of either sex were used.

Western Blot

Western blots were performed as described in Santiago-González et al. (2017). Proteins (20μg/line) were separated using NuPAGE® Novex® 4–12% Bis-Tris Protein Gels (Life Technologies). Nonfat milk (5%), tween-20 (0.1%) in PBS was used to block PDVF membranes overnight at 4°C. The same blocking solution was used to dilute the primary antibodies and the membranes were then incubated overnight at 4°C with agitation. Membranes were scanned with a C-Digit Bot Scanner (LI-COR) and protein bands were identified by chemiluminescence using the Amersham ECL kit (GE Healthcare) with horseradish peroxidase-conjugated secondary antibodies (GE Healthcare). Protein bands were quantified using the Image Studio™ Software (LI-COR). Primary antibodies: β-actin

(mouse; 1:1000; Sigma-Aldrich), CNP (mouse; 1:1000; Neo-Markers), MBP (mouse; 1:1000; Bio- Legend), MOG (mouse; 1:1000; Millipore), PLP (rat; 1:500; AA3 - PLP/DM20) and p84 (mouse; 1:10000; Genetex).

RT-PCR

Trizol reagent (Life Technologies) was used to isolate RNA. RNA purity and concentration were estimated by measuring the ratio of absorbance at 260/280nm. cDNA was prepared with 1μg of total RNA using the PrimeScript first strand cDNA Synthesis Kit (Takara) and 2.5μM of oligo(dT). The mRNA samples were then denaturized at 65°C for 5min and reverse transcription was performed at 42°C for a period of 60min. The samples were finally heated at 95°C for 5min. The cDNA was amplified using specific primers and the PCR Platinum Super mix (Life Technologies). The PCR products were identified on a SYBR Safe stained agarose gel, and the bands digitized using a Gel Doc™ EZ System (Bio-Rad).

qPCR

Total RNA was extracted and purified from the cortex of controls and Cp cKO mice as described in the RT-PCR section. Briefly, 500μg of RNA was reverse transcribed using PrimeScript™ 1st strand cDNA Synthesis Kit (Takara). qPCR was performed using a CFX96 Touch Real-Time PCR Detection Systems (BioRad) and SYBR™ Green PCR Master Mix (Applied Biosystems™). qPCR conditions were as follows: polymerase activation 95°C (10min), followed by 40 cycles: denaturation at 95°C (15s); primer annealing/elongation at 60°C (60s). Primer specificity was analyzed adding a melting curve for each reaction. The quantification of the PCR products was performed using the Pfaffl method. Quantities of mRNA were normalized to the housekeeping genes GAPDH and TBP. Six samples per condition were analyzed and primers were designed based on published sequences.

Immunohistochemistry

Mice were perfused with 4% of paraformaldehyde in PBS via the left ventricle and the brains were post-fixed overnight in the same fixative solution at 4°C. Coronal brain slices of 40μm thick were obtained using a vibratome (Leica Biosystems, VT1000-S). Free-floating vibratome sections were incubated in a blocking solution (2% goat serum and 1% Triton X-100 in PBS) for 2h at room temperature and then incubated with the primary antibody overnight at 4°C. Sections were then rinsed in PBS and incubated with Cy3 or Cy5 conjugated secondary antibodies (1:400; Jackson Immuno Research) for 2h at room temperature. Brain sections were mounted on to Superfrost Plus slides (Fisher) using Aquamount (Thermo Scientific). The staining intensity as well as the number of positive cells was assessed in the central area of the corpus callosum (between the midline and below the apex of the cingulum), in the motor and cingulate cortex, and in the dorsal/caudal striatum (immediately underneath the corpus callosum) (Franklin and Paxinos, 2008; Figure 24). The integrated fluorescence intensity was calculated as the product of the area and mean pixel intensity using MetaMorph software (Molecular Devices). For all experiments involving quantification of positive cells and fluorescence intensity in tissue sections, data represent pooled results from at least 4 brains per experimental group. Twenty slices per brain (40μm each) were used and quantification was performed blind to the genotype of the sample using an unbiased stereological sampling method. Primary antibodies: cleaved

(active) caspase-3 (rabbit; 1:1000; Cell Signaling), CC1 (mouse; 1:300; Calbiochem), CD31 (mouse; 1:200; Abcam), GFAP (mouse and rabbit; 1:1000; Dako), Ki67 (rabbit; 1:250; Abcam), Ki67 (mouse; 1:250; BD Biosciences), MBP (mouse; 1:1000; Biolegend), NeuN (mouse and rabbit; 1:100; Millipore), neurofilament M (chicken; 1:2000; Biolegend), Olig2 (mouse and rabbit; 1:500; Millipore), PLP (rat; 1:250, AA3 - PLP/DM20), s100β (rabbit; 1:800; Thermo Scientific) and 8-OHdG (mouse; 1:2000; StressMarq Biosciences).

Electron Microscopy

Mouse brains were perfused transcardially with 3% paraformaldehyde and 1% glutaraldehyde. The body of the corpus callosum at the anterior-dorsal level of the hippocampus was dissected and resin embedded. Thin sections were stained with uranyl acetate and lead citrate and photographed with a FEI Tecnai™ F20 transmission electron microscope as previously described (Cheli et al., 2016). The *g*-ratio was analyzed at least in 200 fibers per animal and the percentage of myelinated axons was determined in 20 randomly selected fields per sample, which resulted in counts of >1000 axons. The *g*-ratio and the percentage of myelinated axons was determined semi-automatically and blind to the genotype of the sample using MetaMorph software (Molecular Devices). For all experimental conditions, data represent pooled results from at least 4 mice.

Perls' Staining

Enhanced Perls' staining was performed as described previously in Cheli et al. (2018). In brief, 20μm coronal brain sections were incubated with 1% H2O2 in methanol for 15min and then with 2% potassium ferrocyanide (pH 1.0) overnight (Iron Stain Kit, Sigma-Aldrich). The reaction was enhanced with 0.025% 3,30-dia- minobenzidine-4Hl, 0.05% H2O2, and 0.005% CoCl2 in 0.1 M PB for 30min. The sections were dehydrated and mounted with Permount. Twenty slices per brain and 4 brains per experimental condition were used. The number of positive cells and the integrated staining intensity in several brain areas were measured using MetaMorph (Molecular Devices).

SHIRPA

The procedure was modified from the original SHIRPA protocol. Home cage behavior (barbering, fighting, freezing, and grooming), general appearance (body weight, fur condition, missing whiskers, eye abnormality, and lesions), and neurological reflexes were evaluated. All behavioral analyses described in this work were performed in 10 mice per experimental group (5 males and 5 females) and were completed blind to the genotype of the animal.

Rotarod

Coordinated motor activity was measured using a rotarod apparatus following the standard procedure of EMPReSS (European Mouse Phenotyping Resource of Standardized Screens http://empress.har.mrc.ac.uk/). Two protocols were used, (1) constant speed: mice were placed on the rod rotating at a constant speed of 20rpm; (2) acceleration protocol: mice were placed on a rod rotating at 4rpm and the speed of rotation was gradually increased up to

40rpm in a 5min time period. The time until the mice fell to the floor of the apparatus was measured. Each mouse was tested three times with approximately 20min between each trial.

Open Field

Mice were placed in the procedure room for at least 2h before the test for adaptation to the new environment. The open field apparatus consisted of a round box (1m diameter) with opaque walls (50cm high) and was placed in indirect light (50 lx). The mice attached to the swivel unit were gently placed in the open field facing the opaque walls and allowed to freely explore the apparatus for 10min. The total distance traveled, the number of crosses, the time spent in the center area (60cm diameter), and the number of rearings were automatically recorded using a video camera system. The apparatus was cleaned with 70% ethanol between subjects.

Novel Object Recognition

Mice underwent three sessions separated by 24h to evaluate their ability to recognize a novel object from a familiar one in a round plastic box. In the first trial, animals were placed in an empty arena (a rectangular box; the same one used in the open field analysis) and allowed to explore the environment for 10min. Twenty-four hours later, animals were put back in the box for the training session where they were exposed to two identical objects located in two equidistant areas of the box. The exploration time of each object was recorded using a video camera system. After 24h, mice were returned to the box to start the testing round where they were exposed to one familiar object and one novel object, which was different from the familiar one in color and shape. The interaction times with the familiar object (Tf) and the novel object (Tn) were used to determine the interaction index [Tn/(Tn+Tf)]. Interaction was defined as facing (within 2cm of the object) or touching the object. The chamber and objects were thoroughly cleaned with 70% alcohol after every session.

Social Interaction

The testing apparatus consisted of a rectangular, three-chambered box and a lid with a video camera. Each chamber was 20×40×22cm and the dividing walls were made from clear Plexiglas with small square openings (5×3cm) allowing access into each chamber. An unfamiliar mouse (stranger 1), which had had no prior contact with the subject mouse, was placed in one of the side chambers. The location of stranger 1 in the left versus right side chamber was systematically alternated between trials. The stranger mouse was enclosed in a small, round wire cage, which allowed nose contact between the mice but prevented fighting. The cage consisted of vertical bars separated by 0.5cm and was 11cm in height with a bottom diameter of 9cm. The subject mouse was first placed in the middle chamber and allowed to explore the entire box for 10min. The amount of time spent in the empty chamber (E) and the chamber where the stranger 1 was placed (S1) was measured with the aid of a camera fitted on top of the box. Each mouse was tested in a 10min session to quantify the social preference index S1/(S1+E). After the first 10min session, a second unfamiliar mouse was placed in the chamber that had been empty during the first 10min session. This second stranger was also enclosed in an identical small wire cage. The test mouse thus had a choice between the first, already-investigated unfamiliar mouse (stranger 1) and the novel unfamiliar mouse (stranger 2). The amount of time spent interacting

with stranger 1 (S1′) and stranger 2 (S2) was measured for determination of the social recognition index S2/(S2+S1′).

Statistical Analysis

The Kolmogorov–Smirnov test was used to confirm the normal distribution of all data sets. Single between-group comparisons were made using unpaired t-test (Student's t test), using a confidence interval of 95%. Multiple comparisons were investigated by one-way ANOVA followed by Bonferroni's multiple comparison test. The *g*-ratio distribution analysis was done using a simple linear regression model with a confidence interval of 95%. GraphPad Prism (GraphPad Software) was used to perform all the statistical tests. A value of $p<0.05$ for two-tailed test was the criterion for significant differences between experimental groups. For all the experiments, data represent pooled results from at least four brains per experimental group.

RESULTS

Conditional deletion of astrocytic Cp during development

Conditional knockout mice for the Cp gene in astrocytes were created by crossing the Cp floxed line with the Glast1*Cre*ER^{T2} mouse. The Glast1*Cre*ER^{T2} transgenic mice restricts the expression of the *Cre* recombinase exclusively to Glast1-positive astrocytes of the postnatal brain (Trans et al., 2018; Cheli et al., 2021). To induce *Cre*-mediated recombination, **Control** (*Cre*-negative) and **Cp cKO** (Cp$^{f/f}$, Glast1*Cre*ER$^{Cre/-}$) littermates were injected with tamoxifen for five consecutive days starting at postnatal day 2 (P2) and brains were collected at three different time-points: P15, P30, and P60 (Figure 1A). RT-PCR analysis were conducted with total cortical mRNA to confirm *Cre*-mediated recombination of the Cp gene (Figure 1B). Additionally, cell specificity was evaluated by crossing the Glast1*Cre*ER^{T2} mouse with the *Cre* reporter line Ai9(RCL-tdT). Figure 1C shows the expression of the *Cre* reporter fluorescent protein tdTomato in cortical and callosal astrocytes at P15. tdTomato-positive cells in the cortex, corpus callosum, and striatum exhibited the normal astrocytic morphology, and more than 60% of these cells were positive for GFAP in all brain areas (Figure 1D). Additionally, most tdTomato-positive astrocytes were in close contact with blood vessels (CD31-positive structures) and less than 1% of these cells were positive for Olig2 (Figure 1C and D). Figure 1E shows the distribution of tdTomato-positive astrocytes in a coronal brain slice at P60, also confirming an efficient *Cre* recombination at this time-point.

To determine the effect of astrocytic Cp deletion in postnatal myelination, immunohistochemical experiments for myelin proteins were performed on coronal brain slices. As shown in Figures 2A–D, significant reductions in the fluorescence intensity of MBP and PLP were observed in Cp cKO mice at all time-points. Interestingly, this hypomyelination was found to be more pronounced in older animals. These results were further confirmed by western blot analysis for myelin proteins at P15 (Figure 2E) where the expression of MBP, CNP, PLP, and MOG was decreased in Cp cKO brains. The myelin thickness and the proportion of myelinated axons were additionally analyzed by electron microscopy in the body of the corpus callosum (Figure 3). Throughout postnatal

development, Cp cKO animals presented an important increase in the mean *g*-ratio of myelinated axons (Figure 3B and C) and a reduction in the percentage of myelinated axons (Figure 3E).

The density and maturation of oligodendrocytes were examined in several brain areas throughout the postnatal development of the Cp cKO mouse. The transcription factor Olig2, which is localized to the oligodendrocyte nucleus at all developmental stages (Meijer et al., 2012), as well as the somatic marker CC1, which is restricted to myelinating oligodendrocytes (Bin et al., 2016), were utilized to measure total and mature oligodendrocytes, respectively. Both the cortex and the corpus of Cp knockout mice presented a significant decrease in the total number of oligodendrocytes (Olig2-positive cells) (Figure 4A and B) and in the population of mature myelinating (CC1-positive) cells (Figure 4C and D). In congruence with our myelin protein findings, these reductions were greater in older Cp cKO mice (Figure 4A–D). Overall, the percentage of Olig2/CC1 double-positive cells was significantly reduced in Cp cKO brains in both the cortex and corpus callosum (Figure 4E and F). To measure oligodendrocyte proliferation, brain slices were stained with Olig2 and the mitotic marker Ki67. Although we found no changes in the corpus callosum, the number of proliferating oligodendrocytes (Olig2-Ki67 double-positive cells) was increased in the cortex of Cp cKO animals at all time-points (Figure 4G and H).

A series of immunohistochemistry experiments were completed to study astrocyte numbers, distribution, and proliferation. No statistical changes were found in the number of s100-positive astrocytes (Figure 5A and B). However, conditional knockout mice did show a decrease in the number of double-positive cells for s100 and Ki67 in cortical areas (Figure 5C and D) as well as a reduction in the density of GFAP-positive astrocytes in both the cortex and corpus callosum at P15 (Figure 5E and F). The Perls' staining technique, which detects ferric iron depositions in tissue samples, was performed to examine iron distribution in Cp cKO brains (Figure 6). Cp cKO animals showed fewer positive cells and less tissue staining intensity than controls in both the cortex and corpus callosum at all time-points except P15 (Figure 6A, B and C). To measure intracellular iron quantities in specific cell types, Perls' staining intensity was determined in oligodendrocytes of the corpus callosum and neurons of the upper layers of the somatosensory cortex (Figure 6D and E). The average Perls' staining intensity in cortical neurons was found to be normal (Figure 6D and E); however, oligodendrocytes situated in the corpus callosum of Cp cKO animals showed a clear reduction in the iron staining intensity (Figure 6D and E). According to the anatomical distribution and shape of iron-positive cells, these data suggest an oligodendrocyte-specific iron deficiency (Figure 6D and E).

Immunohistochemical experiments were done to evaluate neuronal development and to measure the extent of oxidative stress in Cp cKO brains. NeuN and neurofilament M were used to measure neuronal numbers and morphology, and 8-hydroxy-2'-deoxyguanosine (8-OHdG)—a specific antibody that interacts with repair products of oxidized guanine lesions (Kasai and Nishimura, 1983)—was used to study DNA and RNA damage associated to oxidative stress. While no significant changes were found in cortical thicknesses or number of NeuN-positive cells (Figure 7A and B), a statistical decline in the intensity of neurofilament M was observed in all cortical layers of the P60 Cp cKO brain (Figure 7B).

Furthermore, an increase in 8-OHdG signal was detected in all Cp cKO brain areas at P30 and P60 (Figure 7A and C). Although there were no changes in 8-OHdG DNA and RNA oxidation in GFAP-positive astrocytes, greater staining intensity was observed in neurons (NeuN/8-OhdG double-positive cells) and oligodendrocytes (Olig2/8-OHdG double-positive cells) of Cp cKO brains (Figure 7A and D). In the cortex of Cp cKO mice, levels of several antioxidant enzymes were analyzed by qPCR (Figure 7E). In contrast with the histological results, the expression levels of superoxide dismutase (SOD), glutathione peroxidase (GPX), and the stress-induced heme oxygenase-1 (HO-1) were normal or slightly diminished in the cortex of Cp-deficient mice at P60 (Figure 7E). Additionally, apoptotic cell death was investigated by staining for the activated form of Caspase-3. The combination of this marker with NeuN, Olig2, and GFAP reveals no changes in the survival of neurons, oligodendrocytes, or astrocytes at any developmental time-point (Figure 7F).

The role of astrocytic Cp in the aging brain

To explore the function of astrocytic Cp in the aging brain, **Cp cKO** ($Cp^{f/f}$, Glast1*Cre*$ER^{Cre/-}$) and **Control** (*Cre*-negative) littermates were injected with tamoxifen at 8 months of age and brains were collected for analysis at 12 and 18 months (Figure 8A). Figure 8B shows a representative RT-PCR experiment for cortical RNA isolated at 12 months. Both the presence of the truncated Cp mRNA and reduction in the normal Cp transcript confirm an effective *Cre*-mediated recombination in Cp cKO samples (Figure 8B). First, myelin integrity was examined in these aged animals via immunohistochemistry and western blot for myelin proteins. Relative to controls, MBP and PLP expression was substantially decreased in the cortex, corpus callosum, and striatum of Cp cKO mice (Figure 8C, D, E and F). A similar decrease was seen via western blot analysis for myelin proteins (Figure 8I). Oligodendrocyte numbers and maturation were also investigated using the specific markers Olig2 and CC1. The amount of cortical Olig2- and CC1-positive cells was normal in 12-month-old Cp cKO mice; however, a significant reduction in the density of Olig2- and CC1-positive oligodendrocytes was evident in the cortex of Cp cKO brains at 18 months (Figure 8G and H). Oligodendrocyte proliferation was also analyzed in these animals by combining Olig2 with the mitotic marker Ki67. At both time-points, the number of proliferating Olig2-positive cells in Cp cKO brains was equal to control levels (Figure 8H). In agreement with the reduction in myelin proteins seen via immunohistochemistry and western blot, electron microscopy analysis in the central portion of the corpus callosum revealed a reduced percentage of myelinated axons and a clear increase in the *g*-ratio of myelinated fibers in Cp cKO mice (Figure 9A and B). Additionally, the proportion of axons with signs of active degeneration such as axonal swelling, dysmorphic mitochondria, autophagic vacuoles, and abnormal myelin sheaths, was increased in Cp cKO samples (Figure 9C and D).

Ferric iron deposition in the brain of aged Cp cKO mice was assessed by the Perls' histochemical technique (Figure 9E and F). In contrast to young cKO animals, aged Cp-deficient subjects displayed more iron-positive cells and greater iron staining intensity than controls in both the cortex and corpus callosum (Figure 9E and F). Enhanced iron reactivity was also found in the striatum and substantia nigra of Cp cKO brains (Figure 9I). Additionally, the specific analysis of callosal oligodendrocytes and cortical neurons of

the Cp cKO brain revealed iron accumulation in both cell types (Figure 9G and H). NeuN signal was used to measure the thickness of the somatosensory cortex and to estimate the density of neurons in all cortical layers of aged Cp cKO brains. Though the morphology of the somatosensory cortex and the density of NeuN-positive cells were normal in 12-month-old Cp cKO animals, 18-month-old Cp-deficient mice showed a clear reduction in the cortical thickness and in the number of cortical neurons (Figure 10A and B). The expression of neurofilament M was also decreased in Cp cKO cortical areas (Figure 10B). Moreover, an increase in 8-OHdG signal was detected in Cp cKO samples, specifically at 18 months (Figure 10C). Similar to what we found in younger Cp cKO mice, 8-OHdG DNA and RNA oxidation was increased in neurons (NeuN/8-OhdG double-positive cells) and oligodendrocytes (Olig2/8-OHdG double-positive cells), but not in astrocytes (GFAP/8-OHdG double-positive cells) (Figure 10A and D). Supporting these data, the expression of several antioxidant enzymes (SOD, GPX, HO-1) was found to be increased in the cortex of Cp cKO at 18 months (Figure 10E). The number of apoptotic neurons (NeuN/Casp-3 double-positive cells) and apoptotic oligodendrocytes (Olig2/Casp-3 double-positive cells) were also increased in 18-month-old Cp cKO animals (Figure 10F).

Behavioral tests were conducted at 18 months of age. Measures of neuromuscular strength and motor coordination learning did not differ between control and Cp cKO mice. Specifically, grip strength, latency to fall in the wire hang test, and latency to fall off the rotarod did not differ significantly between Cp cKO and control animals (Figure 11A, **all data not shown**). To study locomotor activity, animals were placed into an open field chamber where the number of rearings, time spent in the center, number of crosses, and total distance travelled were automatically recorded for 10min. Relative to controls, Cp cKO mice displayed no significant changes in time spent in the center or in number of crosses, but we did find a significant decrease in the total distance travelled by Cp cKO animals (Figure 11B and C). Next, we examined these animals for learning deficits using the novel object recognition test. Our data show no difference between genotypes, with Cp cKO and control mice having equal ability to discriminate between a novel object and a familiar one (**data not shown**). Finally, social interaction was tested using the Crawley's three-chamber social approach test, which allows the social preference of mice to be quantified by comparing the time spent around a wire cage containing a stranger mouse versus the time spent around an empty cage (Moy et al., 2004). This test allows for assessment of both sociability and a social novelty preference. While no significant effect of genotype was found for the social preference index (Figure 11D), Cp cKO mice showed a clear reduction in the social recognition index (Figure 11E).

DISCUSSION

Ablation of astrocytic Cp during postnatal development induces oligodendrocyte iron deficiency and disrupts brain myelination

We have determined that the expression of Cp in postnatal astrocytes is crucial for normal oligodendrocyte progenitor cell maturation and myelin production. Cp deletion in astrocytes during the first postnatal week produces a clear deficit in myelin synthesis in several brain areas and significantly reduces the percentage of myelinated axons in the corpus callosum.

These changes are likely a consequence of abnormal oligodendrocyte maturation; the number of pre-myelinating and mature oligodendrocytes (CC1-positve cells) were reduced in Cp cKO mice in combination with a decline in the density of total oligodendrocytes (Olig2-positive cells). Since the proliferation and survival of oligodendrocyte progenitor cells was normal at all time-points, our data suggest that the lack of Cp activity in astrocytes is primarily affecting the maturation of young oligodendrocytes. Iron metabolism was also severely affected in the brain of postnatal Cp cKO mice. The iron content of white and grey matter areas was below control levels, and the number of iron-positive cells, which expressed the morphology and the anatomical distribution of oligodendrocytes, was reduced in the cortex as well as in the corpus callosum. Iron uptake by immature oligodendrocytes is a key preliminary step for the final differentiation of these cells (Cheli et al., 2018; 2020; 2021). Iron deficiency during perinatal brain development significantly affects oligodendrocyte maturation causing long-lasting hypomyelination (Wan et al., 2020; Cheli et al., 2020). The lack of Cp activity in astrocytes might cause a reduction in iron release via ferroportin and a subsequent decline in astrocytic iron uptake from endothelial cells (De Domenico et al., 2007). Thus, our results indicate that Cp-deficient astrocytes are disturbing brain iron metabolism during early brain development, inducing iron deficiency in pre-myelinating and myelinating oligodendrocytes.

The ferroportin-Cp complex is the central route for cellular iron efflux and is primarily responsible for the regulation of intracellular iron concentrations (Musci et al., 2014). Cp KO astrocytes exhibit reduced iron efflux, iron overload and oxidative stress *in vitro* (Chen et al., 2019). This indicates that Cp is crucial to prevent iron accumulation in astrocytes and, thus, suggests a protective antioxidant function for this enzyme in the developing and adult CNS (Chen et al., 2019). We found a transient reduction in GFAP-positive cells in the cortex and corpus callosum of Cp cKO mice at P15. Since astrocytes stimulate the myelination process by secreting trophic factors or by providing energy and substrates to myelinating oligodendrocytes (Kiray et al., 2016; Tognatta et al., 2020), this decline in the number of cortical and callosal astrocytes at P15 may negatively impact myelin synthesis in the postnatal Cp cKO brain. However, the number, distribution, proliferation, and morphology of s100- and GFAP-positive cells, in both white and gray matter areas were completely normal at later time-points. Furthermore, no signs of iron overload or oxidative stress were detected in astrocytes during postnatal development. In the same line, the cortical thickness and density of neurons in the somatosensory cortex of Cp cKO brains were found to be normal across development. Likewise, the iron content of cortical neurons and expression of several antioxidant enzymes in the Cp cKO brain were equivalent to control levels. However, we found a significant reduction in the expression of cortical neurofilament at P60 and signs of enhanced oxidative stress in oligodendrocytes and neurons at P30 and P60. These results indicate that Cp-deficient astrocytes are producing a mild oxidative injury in these cells early during brain development. This may be the result of toxic ferric iron release by Cp-deficient astrocytes, and/or the uptake of alternative and toxic iron sources by oligodendrocytes and neurons (Musci et al., 2014; Chen et al., 2019). Though, these changes were only clear at P60, suggesting that the initial hypomyelination of Cp cKO mice is primarily a consequence of oligodendrocyte iron deficiency and not oxidative stress.

The lack of Cp activity in astrocytes produces demyelination, neurodegeneration, and behavioral abnormalities in aged mice

Aged Cp cKO mice showed demyelination and a reduced number of mature oligodendrocytes in several brain areas. The corpus callosum of these animals reveals a reduction in the percentage of myelinated axons and a clear increase in the *g*-ratio of myelinated fibers at 18 months of age. Additionally, cortical and callosal oligodendrocytes from aged Cp cKO mice displayed iron accumulation, signs of enhanced oxidative stress, and elevated levels of apoptotic cell death. This indicates that mature-myelinating oligodendrocytes of the aging Cp cKO brain likely experience pathological changes, such as iron overload, oxidative stress, and possible mitochondrial dysfunction, which may affect both myelin maintenance and oligodendrocyte survival. Mature oligodendrocytes can be easily damaged and are particularly sensitive to oxidative stress (Roth and Nuñez, 2016). The excessive breakdown of mature oligodendrocytes associated with myelin loss in aged Cp cKO mice may cause the release of redox-active ferrous iron into the brain parenchyma, further enhancing oxidative stress (Lassmann et al., 2012). The subsequent activation of microglia and release of proinflammatory cytokines and ROS by these cells might also precipitate additional oxidative injury in Cp cKO brains (Williams et al., 2012). Thus, astrocytic Cp activity seems to be crucial to protect mature myelinating oligodendrocytes from iron-induced oxidative stress and vital to prevent a cascade of pathological events leading to demyelination, inflammation, and widespread oxidative damage in the aged brain.

Systemic Cp gene knockout results in brain iron overload and neurodegeneration in aged humans and mice (Jeong and David, 2006, Kono and Miyajima, 2006). Pathological findings in the brains of ACp patients have shown iron accumulation in both astrocytes and neurons as well as neurodegenerative changes in the cerebral cortex, basal ganglia, dentate nuclei, and cerebellar cortices (Miyajima, 2003). To date, the proposed molecular mechanisms of nerve damage by iron accumulation are attributed to ROS and free radical formation (Vassiliev et al., 2005; Levi and Finazzi, 2014). Electron microscopy analysis of the aged Cp cKO corpus callosum revealed an increase in the proportion of axons with swelling, dysmorphic mitochondria, autophagic vacuoles, and irregular myelin sheaths. We have also detected reductions in the density of NeuN-positive cells and neurofilament expression in all cortical layers of the aged Cp cKO brain. These abnormalities were combined with reductions in the thickness of the somatosensory cortex and elevated levels of iron depositions, oxidative stress, and apoptotic cell death in cortical neurons. Toxic ferrous iron released by Cp deficient astrocytes can produce free radical formation in neurons and activate a sequence of pathological events causing axonal degeneration and apoptotic cell death (Chen et al., 2019; Santiago González et al., 2021). Additionally, oligodendrocyte iron overload and demyelination might inactivate mechanisms in these cells that provide antioxidant protection and metabolic support to neurons (Mukherjee et al., 2020). The combination of all these factors may certainly precipitate excessive oxidative and metabolic pressure in aged neurons.

We have previously reported that Cp activity in myelinating glial cells is also crucial to prevent oxidative stress and demyelination in the central and peripheral nervous systems (Santiago González et al., 2021). In line with the results presented in this manuscript,

specific ablation of Cp in aged oligodendrocytes induced myelin loss, brain oxidative stress, and cortical degeneration. However, in contrast to astrocytic Cp deletion, the absence of Cp activity in oligodendrocytes do not produce iron overload in aging neurons, suggesting a different mechanism of neuronal injury. These results indicate that iron homeostasis in glial cells and neurons are interconnected and that healthy iron metabolism in oligodendrocytes and astrocytes is crucial for normal neuronal aging. The mechanism by which intracellular iron concentrations are increased in aged neurons and oligodendrocytes of the Cp cKO brain needs to be dissected in future experiments. For instance, it will be essential to understand if iron accumulation in these brain cells is a primary or secondary event (Texel et al., 2008; 2011). However, there is converging evidence that Cp may play a neuroprotective role in neurodegenerative diseases. Iron chelation or peripheral infusion of Cp can attenuate the neurodegeneration and brain iron elevation in animal models of Parkinson's and Alzheimer's disease (Ayton et al., 2013a; 2014; You et al., 2015). For instance, peripheral infusion of Cp significantly attenuates neurodegeneration and nigral iron accumulation in a mouse model of Parkinson's disease (Ayton et al., 2013b). Thus, Cp upregulation, or supplementation, may be a potential disease-modifying therapy for neurodegenerative diseases associated with brain iron accumulation.

We found that aged Cp deficient mice travelled short distances in the open field and displayed a substantial reduction in the social recognition index. Thus, aged Cp cKO animals exhibit alterations of executive-level processes, such as short-term memory. In agreement with our results, Li and collaborators (2022) have recently shown that Cp deletion in GFAP-positive astrocytes induces learning and memory deficits, reductions in synapse density, and abnormal hippocampal neurogenesis in adult mice. However, they found improved learning and memory functions and reduced brain iron levels in aged Cp-deficient animals (Li et al., 2022). In our experiments, Cp deletion was induced at specific time-points and was restricted to only Glast1-positive astrocytes of the postnatal brain (Tran et al., 2018; Cheli et al., 2021). In contrast, in the work of Li et al (2022) Cp was ablated in all GFAP-positive cells from embryonic stages, potentially creating compensatory effects in aged astrocytes (Malatesta et al.,2003 Garcia et al., 2004; Imura et al., 2003). In summary, we have ablated the Cp gene specifically in astrocytes of the CNS; thus, all the phenotypic changes found in our Cp cKO mouse can be attributed to the absence of Cp activity exclusively in astrocytes. This confirms the central role of astrocytes in brain iron metabolism during both postnatal development and aging, and suggests that brain iron accumulation and neurodegeneration in advanced ACp is primarily a consequence of Cp deficiency in astrocytes.

Acknowledgements:

National Institute of Neurological Disorders and Stroke (award number: 2R01NS078041) and The Legacy of Angels Foundation.

REFERENCES

Abbott NJ, Rönnbäck L, Hansson E (2006). Astrocyte-endothelial interactions at the blood-brain barrier. Nat Rev Neurosci 7: 41–53. [PubMed: 16371949]

Amiry-Moghaddam M, Otsuka T, Hurn PD, Traystman RJ, Haug FM, Froehner SC, Adams ME, Neely JD, Agre P, Ottersen OP, Bhardwaj A (2003). An alphasyntrophin-dependent pool of AQP4

in astroglial end-feet confers bidirectional water flow between blood and brain. Proc Natl Acad Sci USA 100: 2106–2111. [PubMed: 12578959]

Ayton S, Lei P, Adlard PA, Volitakis I, Cherny RA, Bush AI, Finkelstein DI (2014). Iron accumulation confers neurotoxicity to a vulnerable population of nigral neurons: implications for Parkinson's disease. Mol Neurodegener 9: 27. [PubMed: 25011704]

Ayton S, Lei P, Bush AI (2013a). Metallostasis in Alzheimer's disease. Free Radic Biol Med 62: 76–89. [PubMed: 23142767]

Ayton S, Lei P, Duce JA, Wong BX, Sedjahtera A, Adlard PA, Bush AI, Finkelstein DI (2013b). Ceruloplasmin dysfunction and therapeutic potential for Parkinson disease. Ann Neurol 73: 554–559. [PubMed: 23424051]

Bento I, Peixoto C, Zaitsev VN, Lindley PF (2007). Ceruloplasmin Revisited: Structural and functional roles of various metal cation binding sites. Acta Crystallogr D Biol Crystallogr 63: 240–248. [PubMed: 17242517]

Bin JM, Harris SN, Kennedy TE (2016) The oligodendrocyte-specific antibody CC1 binds Quaking 7. J Neurochem 139: 181–186. [PubMed: 27454326]

Breuer W, Hershko C, Cabantchik Z (2000). The importance of non-transferrin bound iron in disorders of Iron Metabolism. Transfusion Science 23: 185–192. [PubMed: 11099894]

Cheli VT, Correale J, Paez PM, Pasquini JM (2020). Iron metabolism in glial cells, consequences for myelination and remyelination. ASN-Neuro 12: 1–15.

Cheli VT, Santiago Gonzalez DA, Marziali LN, Zamora NN, Guitart ME, Spreuer V, Pasquini JM, Paez PM (2018) The divalent metal transporter 1 (DMT1) is required for iron uptake and normal development of oligodendrocyte progenitor cells. J Neurosci 38: 9142–9159. [PubMed: 30190412]

Cheli VT, Santiago González DA, Namgyal Lama T, Spreuer V, Handley V, Murphy GG and Paez PM (2016) Conditional deletion of the L-type calcium channel Cav1.2 in oligodendrocyte progenitor cells affects postnatal myelination in mice. J Neurosci 36: 10853–10869. [PubMed: 27798140]

Cheli VT, Santiago González DA, Wan Q, Denaroso G, Wan R, Rosenblum SL, Paez PM (2021). H-ferritin expression in astrocytes is necessary for proper oligodendrocyte development and myelination. Glia 69: 2081–2998.

Chen Z, Jiang R, Chen M, Zheng J, Chen M, Braidy N, Liu S, Liu G, Maimaitiming Z, Shen T, Dunaief JL, Vulpe CD, Anderson GJ, Chen H (2019). Multi-copper ferroxidase deficiency leads to iron accumulation and oxidative damage in astrocytes and oligodendrocytes. Sci Rep 9: 9437. [PubMed: 31263155]

De Domenico I, Ward DM, di Patti MC, Jeong SY, David S, Musci G, Kaplan J (2007). Ferroxidase activity is required for the stability of cell surface ferroportin in cells expressing GPI-ceruloplasmin. EMBO J 26: 2823–2831. [PubMed: 17541408]

Franklin KBJ, Paxinos G (2008) The mouse brain in stereotaxic coordinates. 3. New York Academic Press.

Garcia AD, Doan NB, Imura T, Bush TG, Sofroniew MV (2004). GFAP-expressing progenitors are the principal source of constitutive neurogenesis in adult mouse forebrain. Nat Neurosci 7: 1233–1241. [PubMed: 15494728]

Hellman NE, Gitlin JD (2002). Ceruloplasmin metabolism and function. Annual Review of Nutrition 22: 439–458.

Imura T, Kornblum HI, Sofroniew MV (2003). The predominant neural stem cell isolated from postnatal and adult forebrain but not from early embryonic forebrain expresses GFAP. J Neurosci 23: 2824–2832. [PubMed: 12684469]

Jeong SY, David S (2003). Glycosylphosphatidylinositol-anchored ceruloplasmin is required for iron efflux from cells in the central nervous system. J Biol Chem 278: 27144–27148. [PubMed: 12743117]

Jeong SY, David S (2006). Age-related changes in iron homeostasis and cell death in the cerebellum of ceruloplasmin-deficient mice. J Neurosci 26: 9810–9819. [PubMed: 16988052]

Kasai H, Nishimura S (1983). Hydroxylation of the C-8 position of deoxyguanosine by reducing agents in the presence of oxygen. Nucleic Acids Symp 12: 165–167.

Kiray H, Lindsay SL, Hosseinzadeh S, Barnett SC (2016) The multifaceted role of astrocytes in regulating myelination. Exp Neurol 283: 541–549. [PubMed: 26988764]

Kono S (2013) Aceruloplasminemia: an update. Int Rev Neurobiol 110: 125–151. [PubMed: 24209437]

Kono S, Miyajima H (2006) Molecular and pathological basis of aceruloplasminemia. Biol Res 39: 15–23. [PubMed: 16629161]

Kono S, Yoshida K, Tomosugi N, Terada T, Hamaya Y, Kanaoka S, Miyajima H (2010). Biological effects of mutant ceruloplasmin on hepcidin-mediated internalization of ferroportin. Biochim Biophys Acta 1802: 968–975. [PubMed: 20655381]

Lassmann H, van Horssen J, Mahad D (2012). Progressive multiple sclerosis: pathology and pathogenesis. Nat Rev Neurol 8: 647–56 [PubMed: 23007702]

Levi S, Finazzi D (2014). Neurodegeneration with brain iron accumulation: update on pathogenic mechanisms. Front Pharmacol 5: 99. [PubMed: 24847269]

Li ZD, Li H, Kang S, Cui YG, Zheng H, Wang P, Han K, Yu P, Chang YZ (2022). The divergent effects of astrocyte ceruloplasmin on learning and memory function in young and old mice. Cell Death Dis 13: 1006. [PubMed: 36443285]

Malatesta P, Hack MA, Hartfuss E, Kettenmann H, Klinkert W, Kirchhoff F, Gotz M (2003). Neuronal or glial progeny: regional differences in radial glia fate. Neuron 37: 751–764. [PubMed: 12628166]

Meijer DH, Kane MF, Mehta S, Liu H, Harrington E, Taylor CM, Stiles CD, Rowitch DH (2012) Separated at birth? The functional and molecular divergence of Olig1 and Olig2. Nat Rev Neurosci 13: 819–31. [PubMed: 23165259]

Miyajima H (2014) Aceruloplasminemia. Neuropathology 35: 83–90. [PubMed: 25168455]

Miyajima H (2003). Aceruloplasminemia, an iron metabolic disorder. Neuropathology 23: 345–350. [PubMed: 14719552]

Miyajima H, Hosoi Y (2018) “Aceruloplasminemia,” in Gene Reviews (Internet), eds Adam MP, Ardinger HH, Pagon RA, Wallace SE, Bean LJH, Stephens K, et al. (Seattle, WA:University of Washington).

Moy SS, Nadler JJ, Perez A, Barbaro RP, Johns JM, Magnuson TR, Piven J, Crawley JN (2004). Sociability and preference for social novelty in five inbred strains: an approach to assess autistic-like behavior in mice. Genes Brain Behav 3:287–302. [PubMed: 15344922]

Muckenthaler MU, Rivella S, Hentze MW, Galy B (2017). A red carpet for iron metabolism. Cell 168: 344–361. [PubMed: 28129536]

Mukherjee C, Kling T, Russo B, Miebach K, Kess E, Schifferer M, Pedro LD, Weikert U, Fard MK, Kannaiyan N, Rossner M, Aicher ML, Goebbels S, Nave KA, Krämer-Albers EM, Schneider A, Mikael Simons M (2020). Oligodendrocytes provide antioxidant defense function for neurons by secreting ferritin heavy chain. Cell Metab 32: 259–272. [PubMed: 32531201]

Musci G, Polticelli F, Bonaccorsi di Patti MC (2014). Ceruloplasmin-ferroportin system of iron traffic in vertebrates. J Biol Chem 5: 204–215.

Patel BN, Dunn RJ, David S (2000). Alternative RNA splicing generates a glycosylphosphatidylinositol-anchored form of ceruloplasmin in mammalian brain. Journal of Biological Chemistry 275: 4305–4310. [PubMed: 10660599]

Price BR, Norris CM, Sompol P, Wilcock DM (2018). An emerging role of astrocytes in vascular contributions to cognitive impairment and dementia. J Neurochem 144: 644–650. [PubMed: 29222909]

Roth AD, Núñez MT (2016) Oligodendrocytes: functioning in a delicate balance between high metabolic requirements and oxidative damage. Adv Exp Med Biol 949: 167–181. [PubMed: 27714689]

Santiago González DA, Cheli VT, Rosenblum SL, Denaroso G, Paez PM (2021). Ceruloplasmin deletion in myelinating glial cells induces myelin disruption and oxidative stress in the central and peripheral nervous systems. Redox Biology 46: 102118. [PubMed: 34474395]

Santiago-González DA, Cheli VT, Zamora NN, Namgyal Lama T, Spreuer V, Murphy GG, Paez PM (2017) Conditional deletion of the L-type calcium channel Cav1.2 in NG2 positive cells delay remyelination in mice. J Neurosci 37: 10038–10051. [PubMed: 28899915]

Sato M, Gitlin JD (1991). Mechanisms of copper incorporation during the biosynthesis of human ceruloplasmin. Journal of Biological Chemistry 266: 5128–5134. [PubMed: 2002050]

Simard M, Nedergaard M (2004). The neurobiology of glia in the context of water and ion homeostasis. Neuroscience 129: 877–896. [PubMed: 15561405]

Texel SJ, Xu X, Harris ZL (2008). Ceruloplasmin in neurodegenerative diseases. Biochem Soc Trans 36: 1277–1281. [PubMed: 19021540]

Texel SJ, Zhang J, Camandola S, Unger EL, Taub DD, Koehler RC, Harris ZL, Mattson MP (2011). Ceruloplasmin deficiency reduces levels of iron and BDNF in the cortex and striatum of young mice and increases their vulnerability to stroke. PLoS One 6:e25077. [PubMed: 21949858]

Tognatta R, Karl MT, Fyffe-Maricich SL, Popratiloff A, Garrison ED, Schenck JK, Abu-Rub M, Miller RH (2020) Astrocytes are required for oligodendrocyte survival and maintenance of myelin compaction and Integrity. Front Cell Neurosci 14: 74. [PubMed: 32300294]

Tran CHT, Peringod G, Gordon GR (2018) Astrocytes integrate behavioral state and vascular signals during functional hyperemia. Neuron 100: 1133–1148. [PubMed: 30482689]

Vashchenko G, MacGillivray RTA (2013). Multi-copper oxidases and human iron metabolism. Nutrients 5: 2289–2313. [PubMed: 23807651]

Vassiliev V, Harris ZL, Zatta P (2005). Ceruloplasmin in neurodegenerative diseases. Brain Res Brain Res Rev 49: 633–640. [PubMed: 16269323]

Wan R, Cheli VT, Santiago González DA, Wan Q, Rosenblum SL, Paez PM (2020) Impaired postnatal myelination in a conditional knock-out mouse for the ferritin heavy chain in oligodendrocyte progenitor cells. J Neurosci 40: 7609–7624. [PubMed: 32868463]

Williams R, Buchheit CL, Berman NE, LeVine SM (2012). Pathogenic implications of iron accumulation in multiple sclerosis. J Neurochem 120:7–25 [PubMed: 22004421]

You LH, Li F, Wang L, Zhao SE, Wang SM, Zhang LL, Duan XL, Yu P, Chang YZ (2015). Brain iron accumulation exacerbates the pathogenesis of MPTP-induced Parkinson's disease. Neuroscience 284: 234–246. [PubMed: 25301748]

SIGNIFICANCE STATEMENT

By knocking-down ceruloplasmin (**Cp**) specifically in astrocytes we have stablished that iron release from these cells via the Cp/ferroportin complex, is crucial for oligodendrocyte iron homeostasis and normal CNS postnatal myelination. Furthermore, astrocytic Cp activity is relevant for myelin maintenance and/or turnover in myelinating oligodendrocytes, as well as to prevent oxidative stress and neurodegeneration in the aging brain.

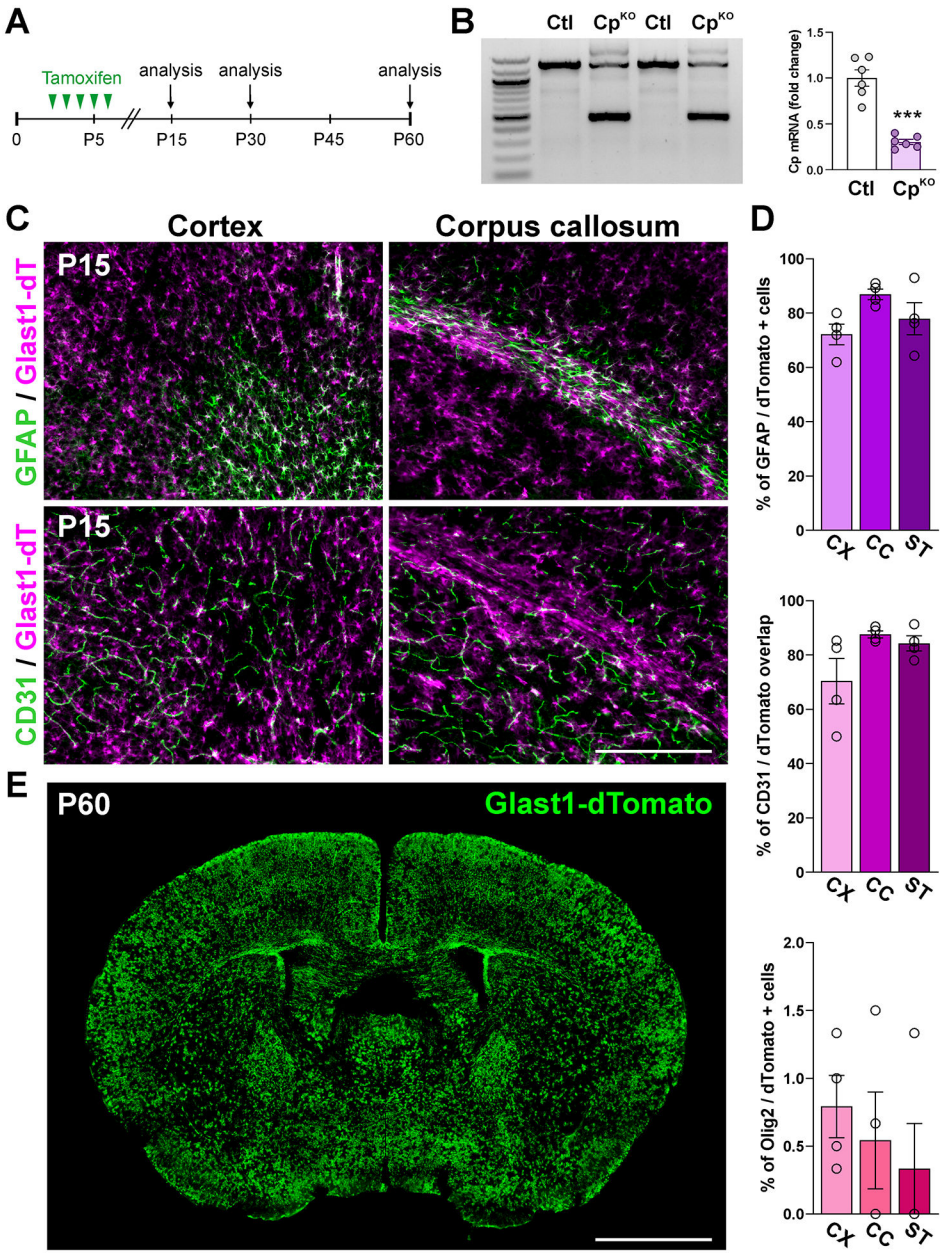

FIGURE 1: Recombination efficacy in the postnatal Cp cKO mouse.

(**A**) Cp cKO mice and control (*Cre*-negative) littermates received five consecutive tamoxifen injections and brain tissue was collected at P15, P30, and P60. (**B**) Semi-quantitative RT-PCR for Cp was performed at P15 with RNA isolated from the brain cortex. Six independent samples per condition were analyzed and Cp mRNA were normalized to GAPDH. Values are expressed as fold change of control values ± SEM. ***p<0.001 vs. controls. Each dot represents the mean of one independent sample. (**C**) GFAP and CD31 immunostaining in the cortex and corpus callosum of Glast1-dTomato mice at P15. Scale bar = 90μm upper panel, 45μm lower panel. (**D**) Percentage of GFAP/ and Olig2/dTomato double-positive cells and overlap between CD31 and dTomato in the somatosensory cortex (CX), lateral corpus

callosum (CC), and striatum (ST). (**E**) Distribution of Glast1-dTomato-positive cells in a coronal brain slice at P60.

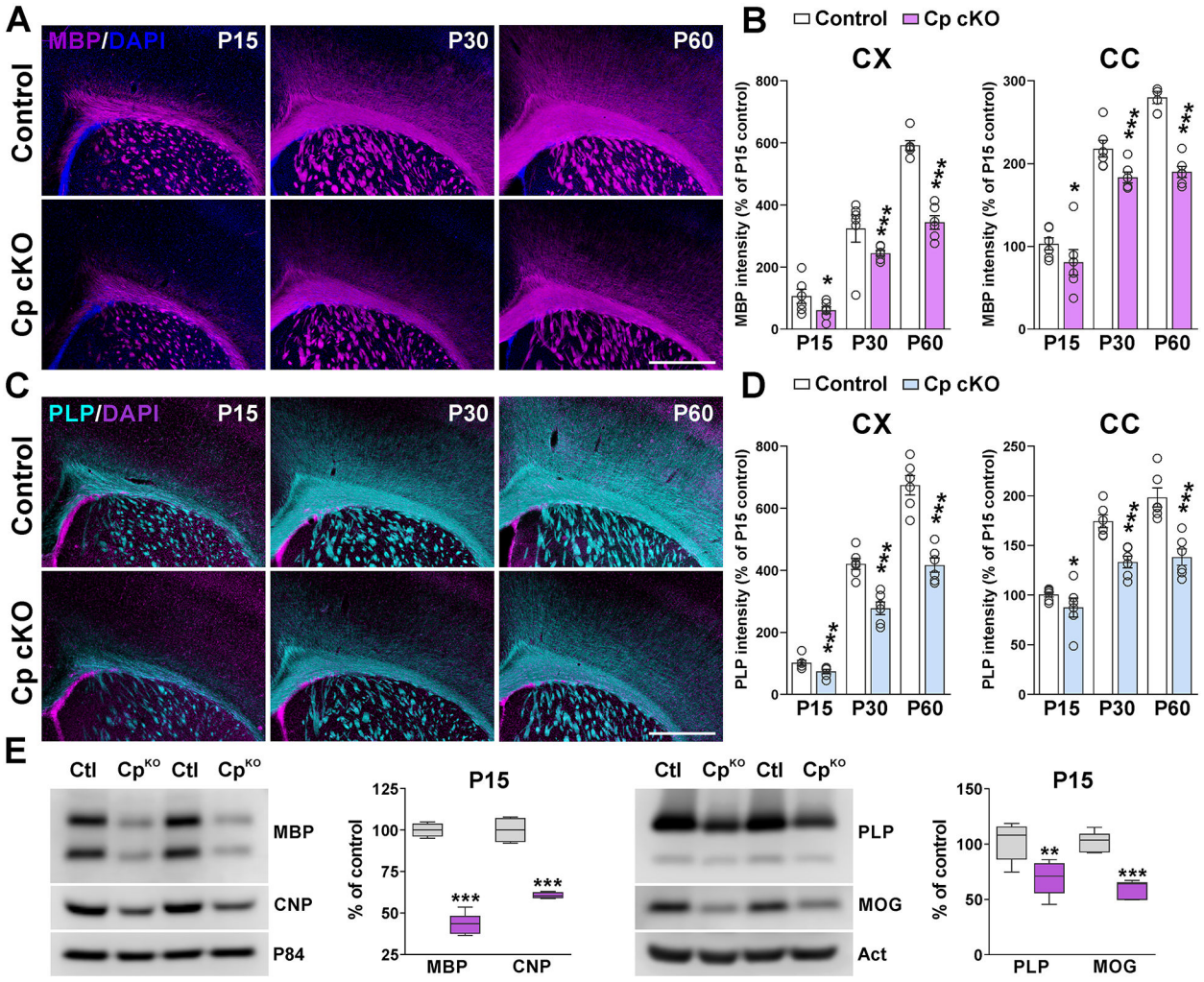

FIGURE 2: Myelin proteins synthesis in the postnatal Cp cKO mouse.

(**A and C**) MBP and PLP immunostaining in Cp cKO brains at P15, P30, and P60. Scale bar = 180 μm. (**B and D**) Integrated fluorescence intensity for MBP and PLP in the cortex (CX) and lateral corpus callosum (CC). Data represent pooled results from at least 4 brains per experimental group and values are expressed as percentage of P15 controls ± SEM. Each dot denotes the mean of one subject. *p<0.05, ***p<0.001 versus respective controls. (**E**) Western blots for MBP, CNP, PLP and MOG in the corpus callosum of Cp cKO animals at P15. P84 and β-actin were used as internal standards and box-and-whisker plots are showing means ± SD from four independent experiments. **p<0.01, ***p<0.001 versus respective controls.

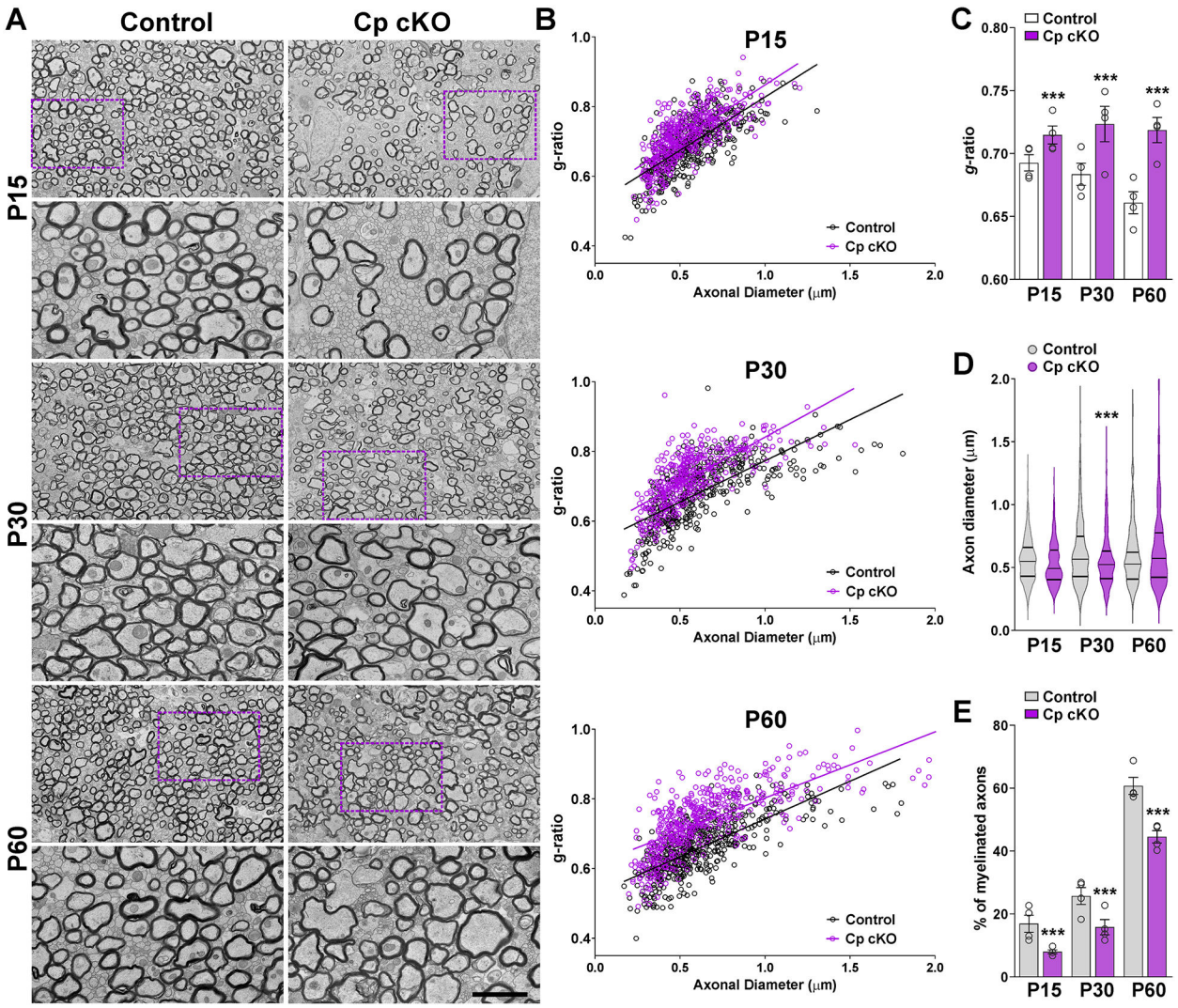

FIGURE 3: Electron microscopy of the Cp cKO corpus callosum.

(**A**) Electron micrographs of axons in the corpus callosum of Cp cKO mice at P15, P30 and P60. Scale bar = 8μm upper panel; 2μm lower panel. (**B**) Scatter plot of *g*-ratio values of myelinated axons. (**C**) Mean *g*-ratio values of myelinated axons for the same experimental conditions. (**D**) Mean axonal diameter of myelinated axons. (**E**) Percentage of myelinated axons. Four animals per experimental group and 200 fibers per mouse were analyzed. Values are expressed as mean ± SEM. ***p<0.001 versus control. In (**C**) and (**E**) each dot represents the mean of one subject.

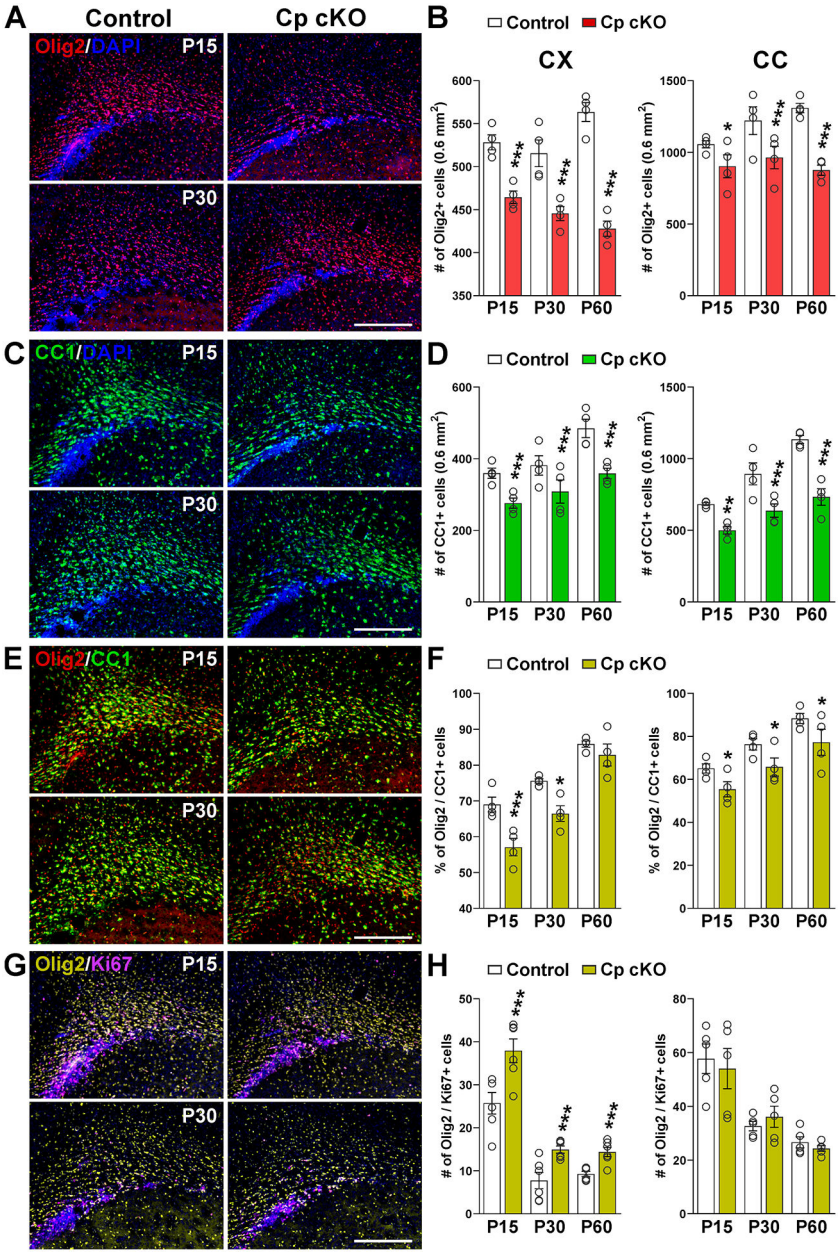

FIGURE 4: Decreased number of mature oligodendrocytes in the Cp cKO CNS.

(**A, C and E**) Coronal brain sections immunostained for Olig2 and CC1 at P15 and P30. Scale bar = 180μm. (**B, D and F**) The number of Olig2 and CC1-positive cells and the percentage of Olig2/CC1 double-positive cells were quantified in the cortex (CX) and lateral corpus callosum (CC) at P15, P30 and P60. Data represent pooled results from at least 4 brains per experimental group and values are expressed as mean ± SEM. *p<0.05, ***p<0.001 vs. respective controls. Each dot represents the mean of one subject. (**G**) Brain sections immunostained for Olig2 and Ki67 at P15 and P30. Scale bar = 90μm. (**H**) Olig2/Ki67 double-positive cells were quantified in the cortex (CX) and lateral corpus callosum (CC) at P15, P30 and P60. Data represent pooled results from at least 4 brains per

experimental group and values are expressed as mean ± SEM. ***p<0.001 vs. respective controls. Each dot denotes the mean of one subject.

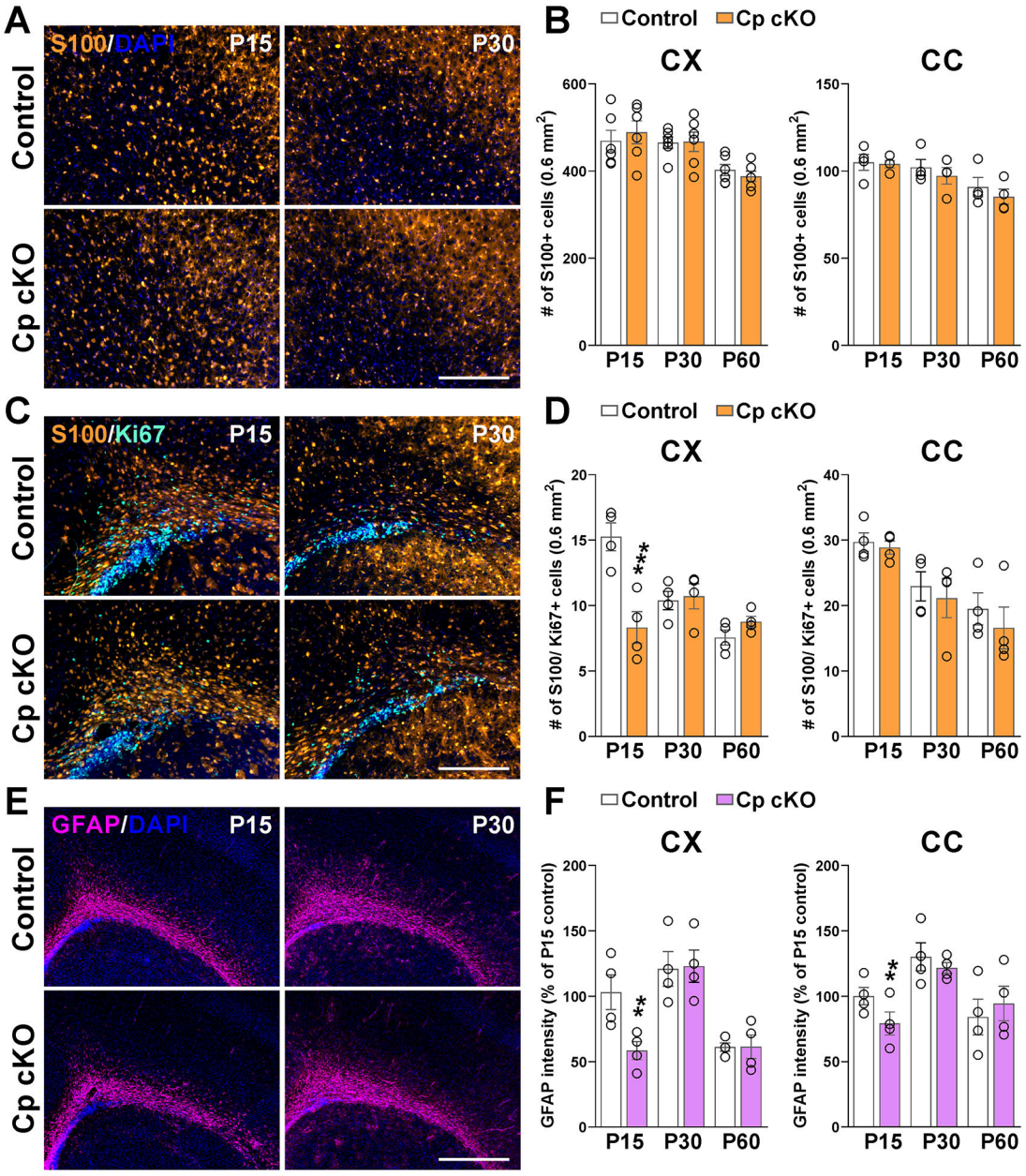

FIGURE 5: Astrocytes numbers in Cp cKO animals.

(**A, C and E**) Coronal brain sections immunostained for s100β, Ki67, and GFAP at P15 and P30. Scale bar = 90μm, A and C; 180μm, E. (**B, D and F**) s100β and GFAP-positive cells, and s100β/Ki67-double positive cells were quantified in the cortex (CX) and lateral corpus callosum (CC) at P15, P30 and P60. Data represent pooled results from at least 4 brains per experimental group and values are expressed as mean ± SEM. **p<0.01, ***p<0.001 vs. respective controls. Each dot denotes the mean of one subject.

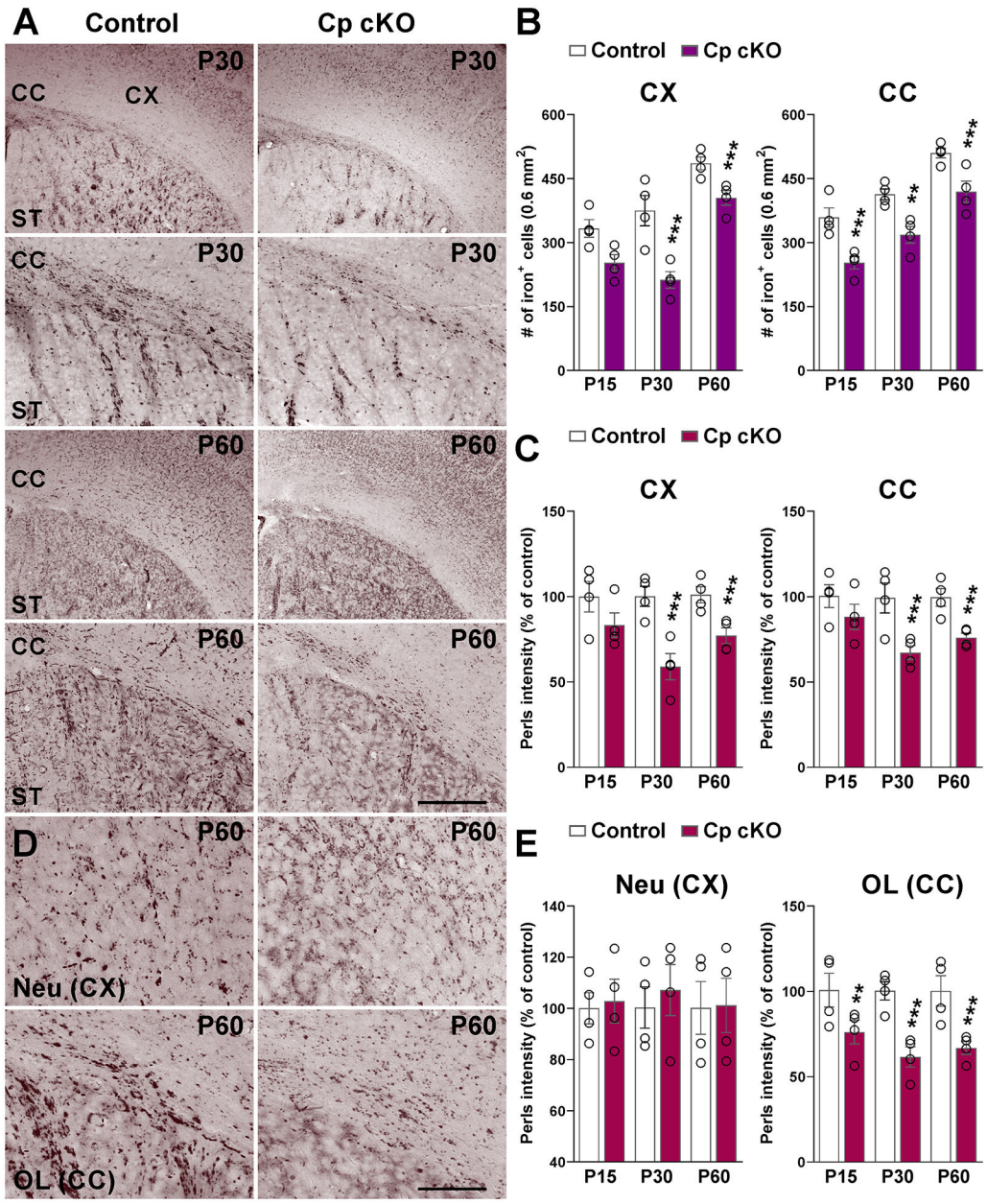

FIGURE 6: Perls' staining in the Cp cKO mice.

(**A**) Perls' staining in coronal brain sections from control and Cp cKO mice at P30 and P60. Scale bar = 180μm upper panel, 90μm lower panel. (**B and C**) Number of Perls' positive cells and average intensity staining in the cortex (CX) and lateral corpus callosum (CC) at P15, P30 and P60. (**D and E**) Average Perls' staining intensity in cortical neurons (Neu CX) and callosal oligodendrocytes (OL CC) at P15, P30 and P60. Scale bar = 45μm. Data represent pooled results from at least 4 brains per experimental group and values are expressed as mean ± SEM. **p<0.01, ***p<0.001 vs. respective controls. Each dot denotes the mean of one subject.

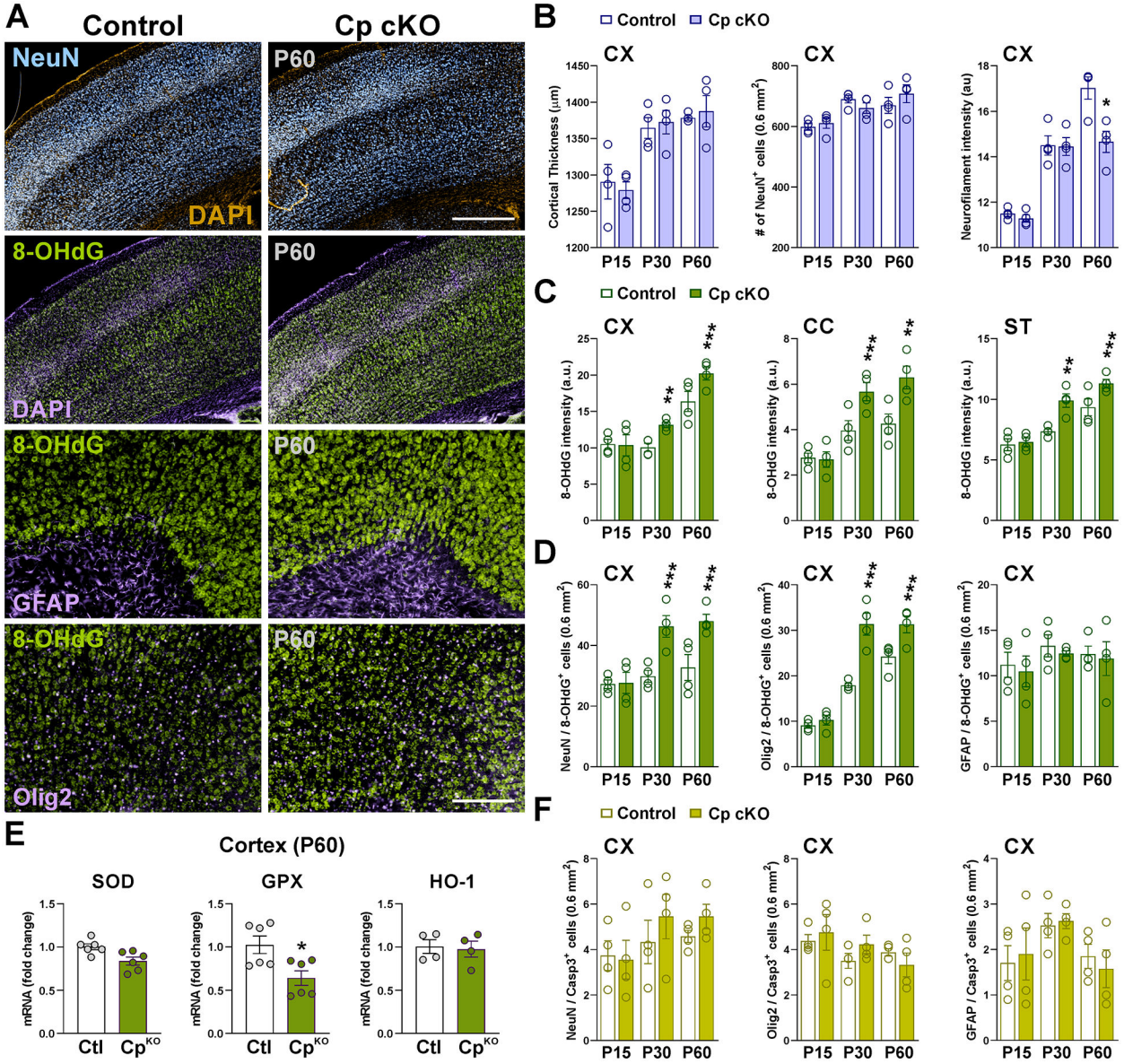

FIGURE 7: Neuronal densities and oxidative stress in young Cp cKO brains.

(**A**) Brain coronal sections from control and Cp cKO brains immunostained for NeuN, 8-OHdG, GFAP, and Olig2 at P60. Scale bar = 180µm upper panels; 90µm lower panels. (**B**) Cortical thickness, total number of NeuN-positive cells, and integrated fluorescence intensity of neurofilament M in the cortex (CX) at P15, P30 and P60. (**C**) Integrated fluorescence intensity of 8-OHdG in the cortex (CX), lateral corpus callosum (CC), and striatum (ST) at P15, P30 and P60. (**D**) Integrated 8-OHdG fluorescence intensity in cortical NeuN-, Olig2-, and GFAP-positive cells. (**E**) qPCRs for superoxide dismutase (SOD), glutathione peroxidase (GPX) and heme oxygenase-1 (HO-1) were performed at P60 with RNA isolated from the cortex of Cp cKO mice. GAPDH and TBP were used as internal standards and values are expressed as fold change of control values ± SEM. Each dot represents the mean of one independent sample. (**F**) NeuN/, Olig2/, and GFAP/active caspase-3 double-positive cells in the cortex (CX) at P15, P30 and P60. Data represent

pooled results from at least 4 brains per experimental group and values are expressed as mean ± SEM. *p<0.05, **p<0.01, ***p<0.001 vs. respective controls. Each dot denotes the mean of one subject.

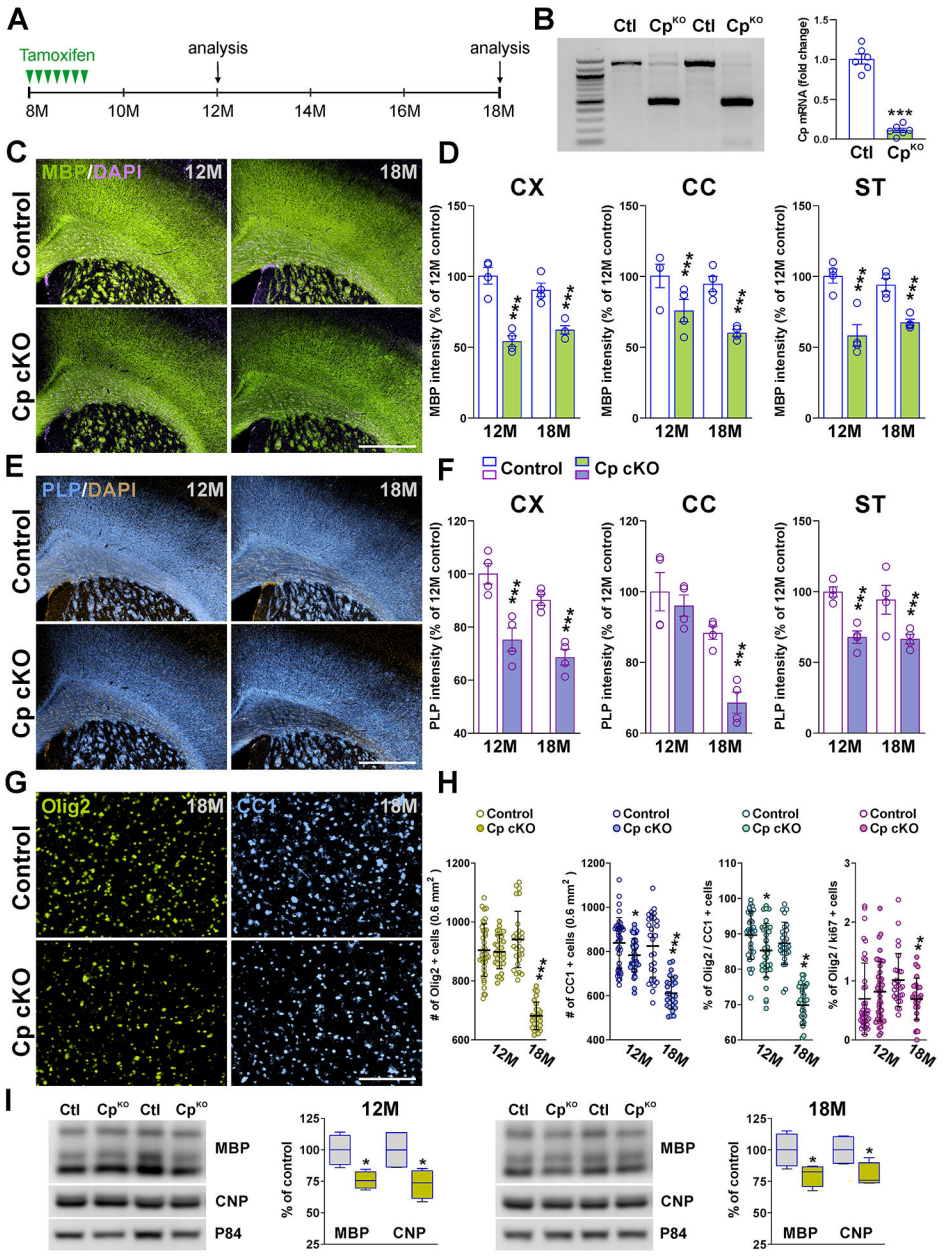

FIGURE 8: Myelin proteins and oligodendrocyte numbers in aged Cp cKO mouse.

(**A**) At 8 months of age Cp cKO mice and control (*Cre*-negative) littermates received seven tamoxifen injections and brain tissue was collected at 12 and 18 months. (**B**) Semi-quantitative RT-PCR for Cp was performed at 12 months with RNA isolated from the brain cortex. Six independent samples per condition were analyzed and Cp mRNA were normalized to GAPDH. Values are expressed as fold change of control values ± SEM. ***p<0.001 vs. controls. Each dot represents the mean of one independent sample. (**C and E**) MBP and PLP immunostaining in the brain of control and Cp cKO mice at 12 and 18 months. Scale bar = 180μm. (**D and F**) Integrated fluorescence intensity for MBP and PLP in the cortex (CX), lateral corpus callosum (CC), and striatum (ST) at 12 and 18 months. (**G**) Cortical sections from control and Cp cKO mice immunostained for Olig2 and CC1 at 18

months. Scale bar = 90μm. (**H**) Olig2 and CC1-positive cells and percentage of Olig2/CC1 and Olig2/Ki67 double-positive cells in the cortex (CX) at 12 and 18 months. Data represent pooled results from at least 4 brains per experimental group and values are expressed as mean ± SEM. *p<0.05, **p<0.01, ***p<0.001 vs. respective controls. Each dot denotes the mean of one subject. (**I**) Western blots for MBP and CNP in the corpus callosum of Cp cKO animals at 12 and 18 months. P84 was used as the internal standard and box-and-whisker plots are showing means ± SD from four independent experiments. *p<0.05 vs. respective controls.

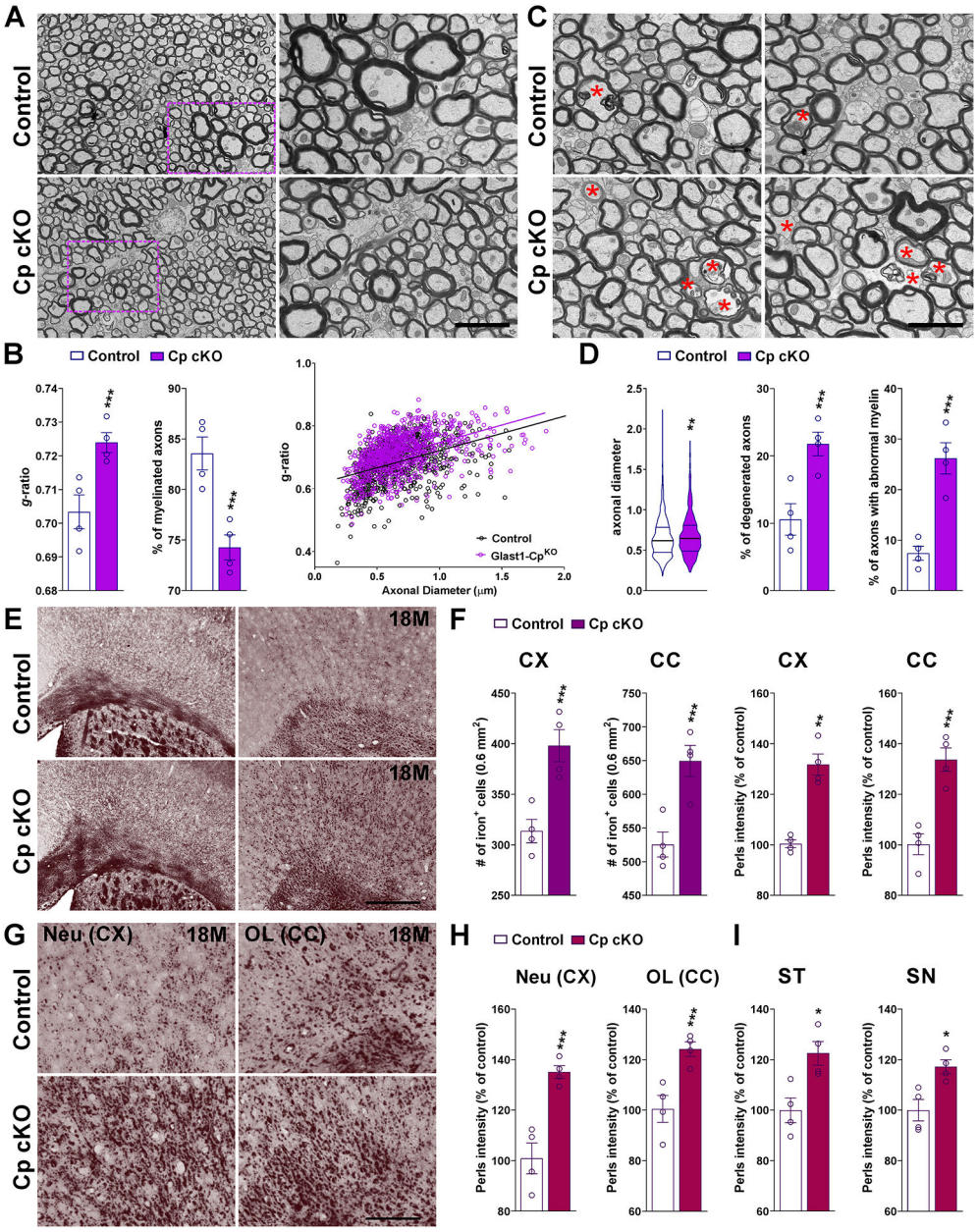

FIGURE 9: Electron microscopy and iron staining in old Cp cKO animals.

(**A**) Electron micrographs of axons in the corpus callosum of Cp cKO mice at 18 months. Scale bar = 8μm left panel; 2μm right panel. (**B**) Mean *g*-ratio values of myelinated axons, percentage of myelinated axons, and scatter plot of *g*-ratio values in control and Cp cKO mice at 18 months. (**C**) Asterisk denotes examples of degenerative axons in the corpus callosum of controls and Cp cKO mice at 18 months of age. Scale bar = 8μm. (**D**) Mean axonal diameter of myelinated axons, percentage of axons with signs of active degeneration, and proportion of axons with abnormal myelin. Four animals per experimental group and 1000 fibers per mouse were analyzed. Values are expressed as mean ± SEM. **p<0.01, ***p<0.001 versus control. Dots in bar graphs represent the mean of one subject. (**E**) Perls' staining in brain sections of control and Cp cKO mice at 18 months. Scale bar = 180μm

left panel, 90μm right panel. (**F**) Number of Perls' positive cells and Perls' intensity staining in the cortex (CX) and lateral corpus callosum (CC) at 18 months. (**G and H**) Average Perls' staining intensity in cortical neurons (Neu CX) and callosal oligodendrocytes (OL CC) at 18 months. Scale bar = 45μm. (**I**) Perls' intensity staining in the striatum (ST) and substantia nigra (SN) at 18 months. Data represent pooled results from at least 4 brains per experimental group and values are expressed as mean ± SEM. **p<0.01, ***p<0.001 vs. respective controls. Each dot denotes the mean of one subject.

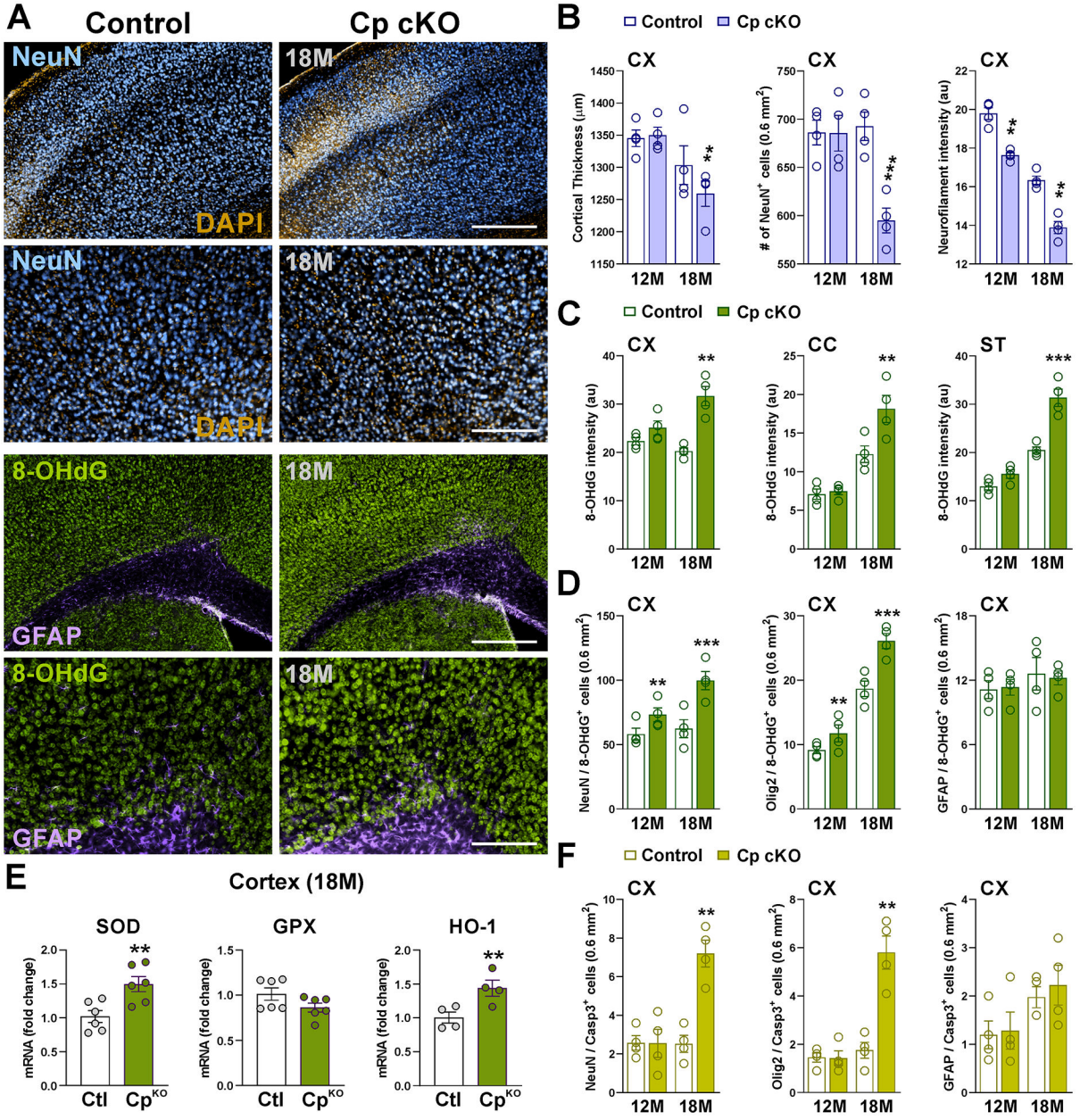

FIGURE 10: Neurodegeneration and oxidative stress in aged Cp cKO brains.

(**A**) Brain coronal sections from control and Cp cKO brains immunostained for NeuN, 8-OhdG and GFAP at 18 months. Scale bar = 180μm upper panels; 90μm lower panels. (**B**) Cortical thickness, total number of NeuN-positive cells, and integrated fluorescence intensity of neurofilament M in the cortex (CX) at 12 and 18 months. (**C**) Integrated fluorescence intensity of 8-OHdG in the cortex (CX), lateral corpus callosum (CC), and striatum (ST). (**D**) Integrated 8-OHdG fluorescence intensity in cortical NeuN-, Olig2-, and GFAP-positive cells. (**E**) qPCRs for superoxide dismutase (SOD), glutathione peroxidase (GPX) and heme oxygenase-1 (HO-1) were performed at 18 months with RNA isolated from the cortex of Cp cKO mice. GAPDH and TBP were used as internal standards and values are expressed as fold change of control values ± SEM. ***p<0.001 vs. controls. Each

dot represents the mean of one independent sample. (**F**) NeuN/, Olig2/, and GFAP/active caspase-3 double-positive cells in the cortex (CX). Data represent pooled results from at least 4 brains per experimental group and values are expressed as mean ± SEM. **p<0.01, ***p<0.001 vs. respective controls. Each dot denotes the mean of one subject.

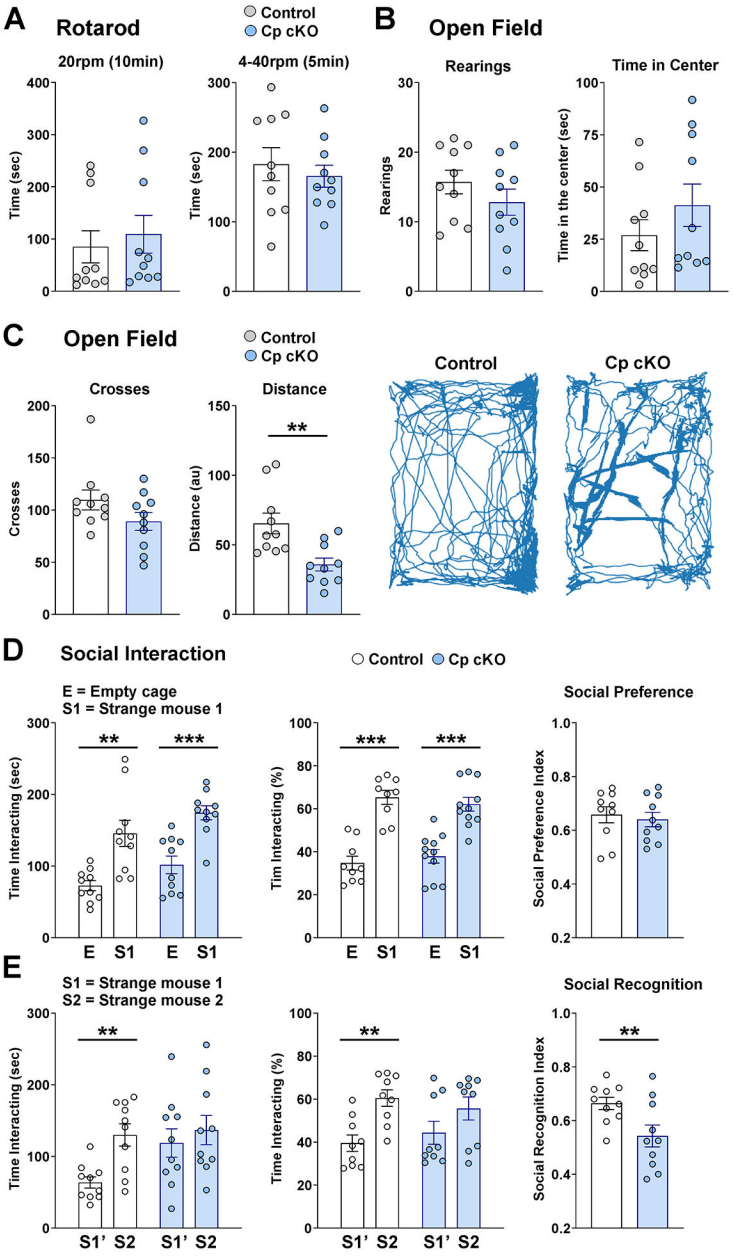

FIGURE 11: Behavioral analysis of aged Cp cKO mice.

(**A**) Controls and Cp cKO mice were tested in the rotarod apparatus using two different settings: constant speed (20rpm) and acceleration (4–40rpm). (**B and C**) Rearings, time in the center, crosses and total travel distance were determined in 18 months-old controls and Cp cKO mice in the open field test. (**D**) Social interaction in control and Cp cKO mice at 18 months. The amount of time interacting with an empty chamber (E) and the chamber containing an unfamiliar mouse (S1) was measured for 10min to estimate the social preference index S1/(S1+E). (**E**) The time spent interacting with the unfamiliar mouse 1 (S1′) and the unfamiliar mouse 2 (S2) was measured in a second session for determination of the social recognition index S2/(S2+S1′). All behavioral analyses were performed in 10 mice per experimental group (5 males and 5 females) and values are expressed as mean ±

SEM. **p<0.01, ***p<0.001 vs. respective controls. Dots in bar graphs represent the mean of one subject.